Journal of Research and Applications in Mechanical Engineering
ISSN: 2229-2152 (Print); 2697-424x (Online)
(2023) Vol. 11, No. 1, Paper No. JRAME-23-11-004
[DOI: 10.14456/jrame.2023.4]

Research Article

Numerical Study of Aeroacoustics for Centrifugal Fan

J. Sriwattanamakin[1,2]
K. Tontiwattanakul[1,2]
C. Chumchan[1,3,*]
N. Moonpa[4]
[1] *Sound and Vibration Research Group, King Mongkut's University of Technology North Bangkok, Bangkok 10800, Thailand*
[2] *Department of Mechanical and Aerospace Engineering, Faculty of Engineering, King Mongkut's University of Technology North Bangkok, Bangkok 10800, Thailand*
[3] *Department of Power Engineering Technology, College of Industrial Technology, King Mongkut's University of Technology North Bangkok, Bangkok 10800, Thailand*
[4] *Mechanics, Materials, and Engineering Design Research Group, Rajamangala University of Technology Lanna, Chiang Mai 50300, Thailand*

Received 23 January 2023
Revised 15 March 2023
Accepted 6 April 2023

Abstract:
Aerodynamic noise is one of the considerable factors in centrifugal fan design. Due to the fact that there are number of parameters involved with a description of a fan's geometry as well as a complex characteristic of airflow, thus bring many difficulties to the study of noise generating mechanism of a centrifugal fan. In this study, the characteristic of fan noise and the outstanding noise source are investigated using an unsteady state flow simulation with an aeroacoustics modelling. Unsteady Reynolds Averaged Navier–Stokes (URANS) and Large Eddy Simulation (LES) are used to predict the derivative of pressure w.r.t. time. Afterward, the acoustic model based on Ffowcs Williams and Hawkings (FW-H) acoustic analogy is applied to calculate monopole and dipole noise sources. Prediction results of aerodynamic noise are compared to an experiment. The results indicate that the surfaces of the blade tips are the dominant tonal noise source, whereas the impeller and volute tongue surfaces are the prominent broadband noise source. Moreover, the characteristic of broadband noise is well predicted by the use of LES coupled with the acoustic model.

Keywords: *Aerodynamic noise, Unsteady Reynold Averaged Navier-Stokes, Large Eddy Simulation, Ffowcs Williams and Hawkings*

1. Introduction

Centrifugal fan is a type of mechanical fan that utilizes the principle of centrifugal force to generate airflow. It plays a significant role in various applications such as ventilation, dust removal, and air conditioning systems. For this reason, this type of fan is widely used in both industry and household sections. However, fan noise is one of the considerable factors, due to the growing demand for reducing noise levels and stringent noise regulations. Therefore, a lot of attention has been paid to the fan noise problem.

Neise [1, 2] reviewed noise reduction methods for a centrifugal fan, and then summarized the effectiveness of these methods. The most significant finding is that interaction between an unsteady flow, which is emitted from the impeller and volute tongue is the dominant Blade Pass Frequency (BPF) noise source.

Ohta and Outa [3] set up the experiment to evaluate and predict the tonal noise generation of the low-specific-speed centrifugal fan. The study showed that the most effective noise source is located close to the volute tongue. Similarly, Velarde-Suarez et al. [4] employed the experimental method to investigate the aeroacoustics behaviour of the

*Corresponding author: C. Chumchan
E-mail address: chartchay.c@cit.kmutnb.ac.th

centrifugal fan. The study confirmed that BPF noise is generated by the interaction between the unsteady flow released from the blade and the volute tongue. On the other hand, Heo et al. [5] stated that the interaction between the incident turbulence and the rotating fan blades is the inflow broadband noise source. They also presented that the interaction between the turbulence components in the boundary layer of the airfoil fan blades and the blades' trailing edge is the broadband self-noise generating mechanism.

In recent years, Hybrid Computational Aeroacoustics (HCAA) has gained widespread use in many engineering applications. Numerous HCAA studies that have been conducted on centrifugal fan noise usually divide into two significant steps. In the first step, the Computational Fluid Dynamics (CFD) method is employed to obtain a noise source from an unsteady near-flow field around the fan. Then, Lighthill's acoustic analogy or its special formulation is applied to calculate a far-field radiated noise based on the noise source that extracts from the unsteady near-flow field. A review of the literature on the utilization of HCAA in the study of fan noise is presented in the following paragraphs.

Zhang et al. [6] applied the URANS with the FW-H acoustic analogy to investigate the aerodynamics and aeroacoustics characteristics of the centrifugal fan. The study indicated that this configuration can be used to capture the BPF and its harmonics noise. The prediction result by Marsan and Moreau [7] showed that the BPF and its harmonics noise are well predicted by the utilization of this configuration. Wu et al. [8] confirmed that this configuration can be applied to capture the evident peak of the BPF and its second harmonic noise.

On the other hand, Chen et al. [9] conducted a combination of LES and FW-H acoustic analogy to predict the aerodynamic noise of the centrifugal fan. The result indicated that the overall trend of the Sound Pressure Level (SPL) and the amplitude of the BPF noise are accurately predicted. The study from Yang et al. [10] confirmed that this configuration can be applied to capture BPF and broadband noise. Kim et al. [11] also showed that the BPF noise and the overall trend of SPL are well predicted by using this configuration.

From the mentioned paragraphs, these configurations appear to be a promising approach for predicting the characteristics of fan noise. However, the FW-H acoustic analogy or its special model calculates the radiated noise based on the noise source extracted from the unsteady near-flow field. Thus, the use of different CFD methods directly influence the fan noise prediction result. There is no study focus on this influence in the context of predicting the noise generated by a centrifugal fan.

The aim of this work is to study the different CFD methods such as URANS and LES coupled with the acoustic model based on FW-H acoustic analogy to predict aerodynamic noise generated by the fan. This study also aims to investigate the characteristic of a low Mach number fan noise and its dominant noise source. In addition, the experimental data is gathered to validate the prediction results from the numerical study.

2. Description of the Investigated Fan

Figure 1(a) represents an isometric view and Fig. 1(b) presents a front view of the investigated fan. Figure 1(b) also shows the casing and the impeller, which are the main components of the fan. The impeller is driven by the brushless direct current electrical motor with adjustable rotational speed between 0 and 7,500 rpm. The fan in this research is classified as a low Mach number machinery since the rotational speed of the fan blades is usually much lower than the speed of sound. However, turbulent flow still occurs in this case and has an impact on the overall aerodynamic noise. The noise emission as specified in the manufacturer's manual is 69 dBA at the rated rotational speed. In addition, the consequential dimensions of the fan are provided in Table 1.

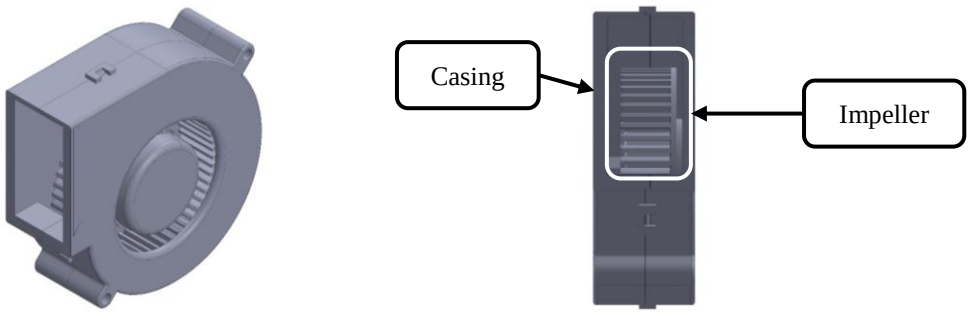

(a) Isometric view (b) Front view

Fig. 1. 3D fan model.

Table 1: Dimension of the investigated fan.

Inlet diameter (mm)	56
Outlet width (mm)	57.6
Inlet diameter of impeller (mm)	56
Outlet diameter of impeller (mm)	70
Volute width (mm)	32.9
Blade width (mm)	1.35
Blade number	52

3. Fan Noise Prediction

3.1 3D Model

A 3D model of the fan was constructed based on the parameters, which are provided in Table 1. To simulate an airflow, a computational domain was divided into a rotational part and a stationary part. Figure 2(a) represents the rotational part, which is defined as the air domain that encloses the impeller. This part is located at the centre of the fan's model and the computational domain. Figure 2(b) presents the stationary part, which is regarded as the air domain that embraces the fan's model, and it has a volume of approximately 8 m^3. An inlet boundary was defined on the left-handed side face of this part, which is located 1 m from the fan's inlet, and on the x-axis direction. Otherwise, all of the other outside faces of this part were set as an outlet boundary.

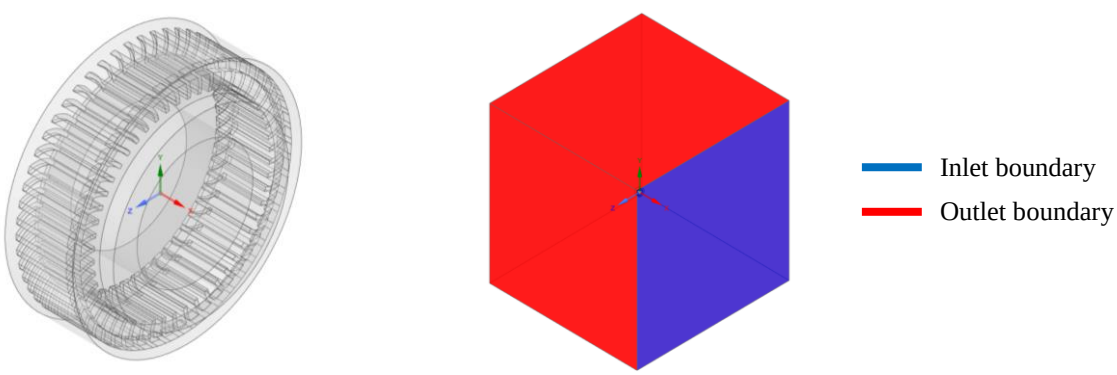

(a) Rotational part (b) Stationary part with defined boundaries

Fig. 2. Computational domain components.

3.2 Mesh Generation

The LES demands a high-resolution grid to resolve the production of turbulence and transition to turbulence directly. Therefore, the poly-hexcore mesh was generated to serve this requirement as well as reduce the number of elements and computational cost [12]. The computational domain was decomposed into hexahedral structural elements and polyhedron unstructured elements as shown in Fig. 3. The prism boundary layer was applied to capture the character of turbulence around the wall of the casing. Moreover, the density of mesh around the impeller is higher than the other areas in the domain.

A grid independent study was carried out to find an optimum total number of elements for a flow field calculation. Five differential total number of element cases were solved by a steady flow simulation. Figure 4 presents the comparison between the magnitude of air velocity at the measurement point, which is located 50 mm from the fan's inlet, and the total number of elements. The result shows that the grid is independent when the total number of elements exceeds 0.8 million. Thus, the case of 1.1 million total number of elements is used for both steady flow and unsteady flow simulations in order to capture the higher resolution of the flow field.

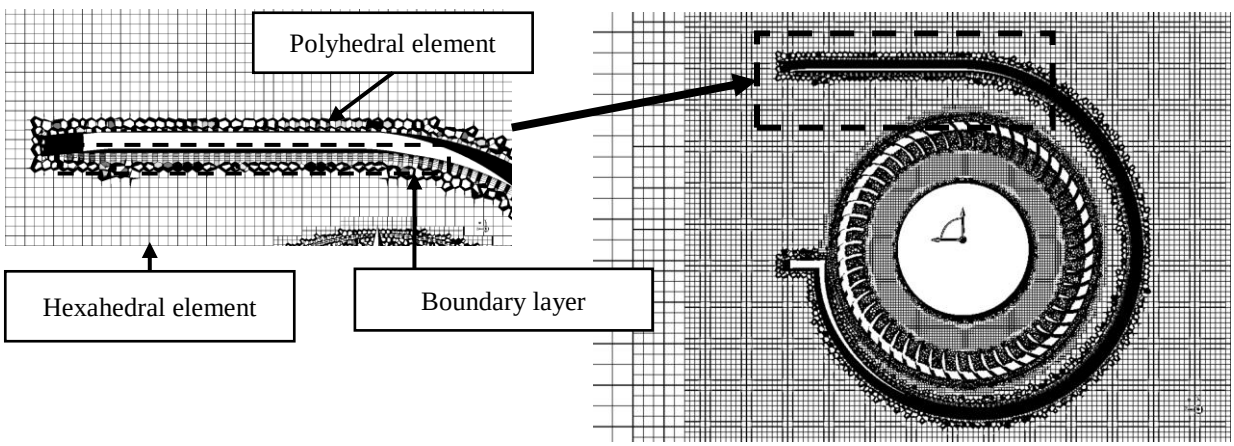

Fig. 3. Detail of mesh generation.

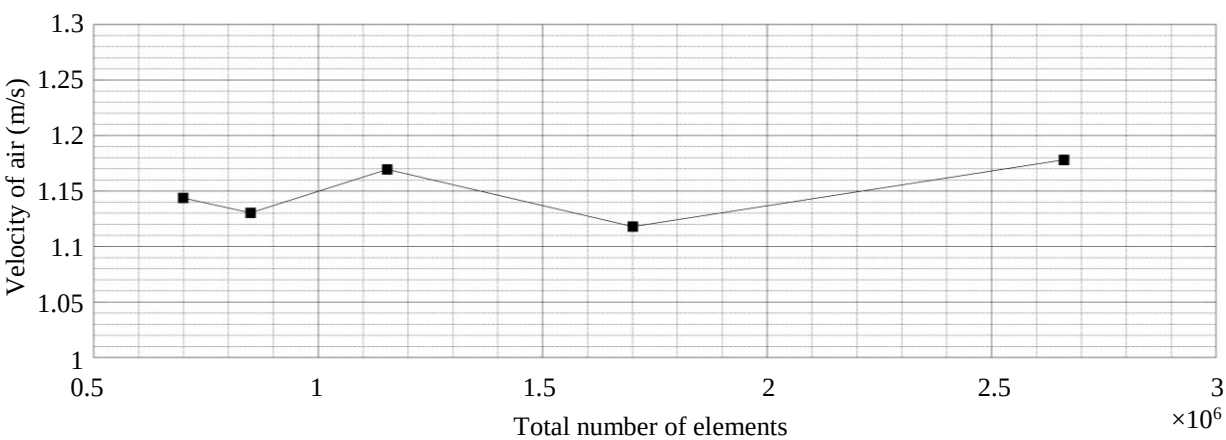

Fig. 4. Result of grid independent study.

3.3 Flow Field Calculation

Flow field calculation was separated into two following steps. Firstly, the steady flow simulation was employed to reduce the computational cost. Its simulation result is also beneficial as an initial condition for the unsteady flow simulation. To account for the effects of curvature, swirl, and rotation, a special k-ε turbulence model was applied. This model is an application of the renormalization group mathematic technique on the k-ε turbulence model, and it

can be denoted as RNG k-ε. A standard logarithmic wall function was also used in the steady flow simulation. The SIMPLEC pressure velocity coupling algorithm was utilized to solve for the pressure field. All discretization schemes were set into second- order upwind for achieving a higher accuracy at the cell face. Then, the unsteady flow simulation was employed to obtain the flow variables, with a particular focus on the derivative of pressure w.r.t. time. This variable indicates the strength of the noise source in an acoustic field. Both RNG k-ε and the LES with the Smagorinsky-Lilly subgrid-scale model were used to simulate the unsteady flow field.

The boundary conditions of the steady flow simulation and the unsteady flow simulation were defined as the same. The boundaries of the stationary part were specified with the static pressure equivalent to atmospheric pressure. At these boundaries, the turbulent intensity was set to 5 percent, and the turbulent viscosity ratio was set to 10. Moreover, the no-slip condition was enforced at all wall boundaries, ensuring that air velocity is restricted to zero at the wall.

The mesh in the rotational part rotates around the x-axis and in the positive direction. The rotational speed of the mesh was set as 7,500 rpm. The grid interface between the rotating and stationary parts based on the sliding mesh technique was applied. A constant timestep of 3.91×10^{-5} s was used in the unsteady flow simulation. The time step was determined based on the highest fan's noise frequencies concerned. To achieve an acceptable residual value, the maximum number of iterations between two time steps was set as 20.

3.4 Fan Noise Calculation

The first acoustic analogy was proposed by Lighthill in 1952 [13, 14]. Navier-Stokes equation is rearranged into terms of noise source and propagating wave. However, this analogy only accounts for the noise generated by turbulent flow. To overcome this limitation, FW-H developed an improved acoustic analogy based on Lighthill's work [15]. This analogy can account for noise generated by a source in relative motion w.r.t. a hard surface and turbulence-generated noise. Due to this capability, the analogy is frequently employed to investigate the characteristic of fan noise. A mathematical expression of FW-H acoustic analogy is written as

$$\frac{1}{c_0^{\,2}}\frac{\partial^2 p'}{\partial t^2}-\nabla^2 p'=\frac{\partial}{\partial t}\{[\rho_0 v_n+\rho(u_n-v_n)]\delta(f)\}-\frac{\partial}{\partial x_i}\{[P_{ij}n_j+\rho u_i(u_n-v_n)]\delta(f)\}+\frac{\partial^2}{\partial x_i\partial x_j}\{T_{ij}H(f)\} \quad (1)$$

in which, c_0 is speed of sound, ρ is fluid density, ρ_0 is free stream fluid density, p' is far-field sound pressure, u_i is fluid velocity component in the x_i direction, u_n is fluid velocity normal to the surface, v_n is surface velocity normal to the surface, and n_j is normal vector of the surface. P_{ij} represents compressive stress tensor, T_{ij} is Lighthill's stress tensor, $\delta(f)$ is Dirac delta function, and $H(f)$ is Heaviside function.

Eq. (1) incorporates three distinct sound sources on its right-hand side. The first term represents a monopole sound source, which is raised from the travelling of the rotating fan blade volume. The second term represents a dipole sound source. This source is generated by unsteady force and pressure fluctuation on the fluid induced by the blade and casing surfaces. The final term is a quadrupole sound source, which is associated with the internal turbulent flow. Due to this study being conducted on the low Mach number fan, the quadrupole sound source is negligible.

To predict the radiated fan noise, the acoustic model based on the combination of free-space Green's function [16] and FW-H acoustic analogy is applied. The fan noise signal at the receiver point, which is located 1 m from the fan's inlet was directly computed through an evaluation of the surface integral. In addition, this model also includes the calculation of the aerodynamic noise that arises due to an external flow around the fan.

4. Fan Noise Measurement

Figure 5 shows a schematic of the equipment setup for the fan noise measurement. Fan noise was measured in an open space that can be classified as an acoustic free-field condition. The fan was positioned on a tripod at the centre of the space and 1.5 m above the floor. To measure the aerodynamic noise, three Bruel & Kjaer type 4958 microphones were introduced in this process. All of them were arranged in an equilateral triangular array to capture a signal from a different direction. The main purpose of using microphone array is to improve the quality of the signal and achieve a reliable measurement result. The array was mounted on the tripod that was located 1 m from the fan's inlet and at the same height as the fan.

In the process of fan noise measurement, a Background Noise (BG) of the space was determined first. To ensure that it was at least 10 dB lower than the fan noise as recommended by ISO 3745 [17]. Then, the fan noise was captured by the microphone array for a duration of 10 seconds. Afterward, the measured signal was then transferred to the Nation Instruments model USB-4431 data acquisition system, which can provide 24-bit data resolution and a sampling rate of 102.4 kHz. The captured acoustic signals were processed using a delay and sum beamforming method [18]. Due to the microphones were located on the same measurement plane, the time delays to be applied to each microphone are zero. Thus, the beamforming output can be calculated using Eq. (2).

$$p_t'(\mathbf{x},t) = \frac{1}{M}\sum_{m=1}^{M} p_m'(\mathbf{x},t) \tag{2}$$

where p_t' is the beamformer output signal from the microphone array, p_m' is the recording signal from the individual microphones, and M denotes the number of microphones.

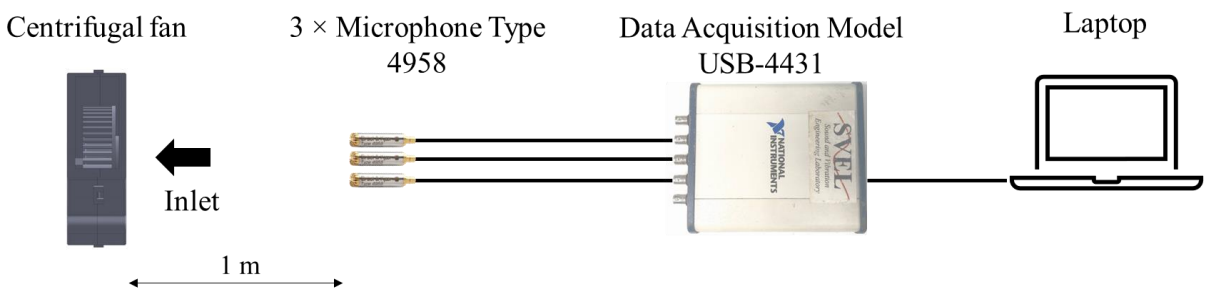

Fig. 5. Schematic of equipment setup.

5. Result and Discussion

5.1 Frequency Spectra

In order to compare predicted and measured results at the same bandwidth of frequency, a low-pass filter was applied. The results were resampled at the same sampling time as the simulation time step, and Fast Fourier Transform was applied to consider these results in the frequency domain. The block size was set as 8,192 points, and the window was set as Hanning with a 67 percent overlap.

Figure 6 represents the SPL spectra of the results within the interested band of frequency, and at the measurement point, which is located 1 m from the fan's inlet. The blue line represents the predicted SPL from the LES coupled with the acoustic model. The obtained SPL from the RNG k-ε coupled with the same acoustic model is illustrated by the red line. The black line shows the SPL of measured fan noise from the microphone array, and the green line is the representation of the BG level in the space. A Root Mean Square Error (RMSE) is utilized to evaluate the accuracy of the predicted SPL against the measured SPL. The formula of RMSE that is used in this study can be mathematically expressed in Eq. (3).

$$RMSE = \sqrt{\frac{1}{P}\sum_{k=1}^{P}(E_k(F) - P_k(F))^2} \tag{3}$$

where P denotes the number of data points, E_k is measured SPL in the frequency domain, and P_k is predicted SPL in the frequency domain.

According to this figure, it can be observed that the predicted SPL obtained from the LES coupled with the acoustic model shows a good agreement with the measured SPL in terms of the broadband noise characteristic. The overall trend of SPL is one agrees, and the RMSE between these two is 7 dBA. Conversely, the predicted SPL obtained from the RNG k-ε coupled with the same acoustic model fails to capture the broadband noise characteristic. In this case, the predicted SPL is significantly lower than the measured SPL and almost the same level as BG. The RMSE between

the predicted and measured SPL is 16 dBA. Thus, it can be claimed that the LES coupled with the acoustic model yields a more precise in prediction of broadband noise.

Due to the analytical solution, the first harmonic of BPF noise occurs at 6,500 Hz. Thus, both LES and RNG k-ε coupled with the acoustic model can be utilized to capture the BPF noise characteristic. However, it must be mentioned that the process of fan noise measurement, which was conducted in this study fails to capture the BPF noise. In fact, the discrepancy in the SPL between the measured fan noise and the measured BG at the BPF surpasses 23 dBA. This issue will be investigated in further study.

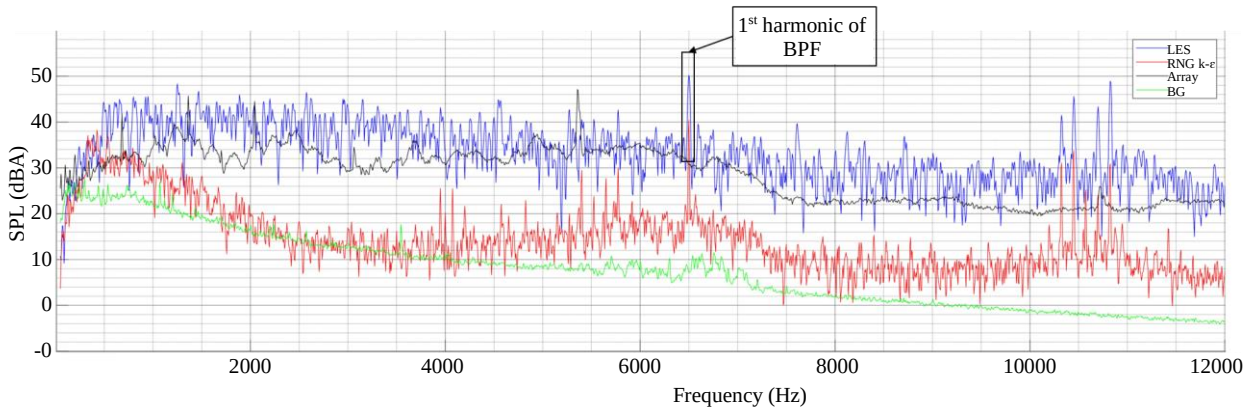

Fig. 6. Predicted and measured SPL.

5.2 Noise Source Identification

One of the conventional units offered by the simulation program to indicate acoustic source strength is the derivative of pressure w.r.t. time. This unit is used to compute the power spectrum on the fan's surfaces in order to determine the power of the noise source. Figure 7 and Figure 8 show the calculated power spectrum at the physical time frame of 0.39 s. The results at 2,000 Hz and 4,000 Hz are selected as a sample to represent the source strength in the broadband noise region, while the result at 6,500 Hz is used to present the source strength at the BPF. The red colour on the surface denotes a high power of noise source in that area, while the blue colour on the surface indicates a relatively low power of noise source compared to other areas.

Figures 7(a), 7(b), 7(c), and 7(d) present the power spectrum computed from LES and RNG k-ε coupled with the same acoustic model at 2,000 Hz and 4,000 Hz, respectively. According to these figures, it can be seen the impeller and volute tongue surfaces are the significant broadband noise source. Due to their calculated power spectrum being higher than other areas. These figures also illustrate that the overall calculated power spectrum by the LES is much higher than the RNG k-ε. Thus, the predicted amplitude of SPL from LES is higher than the RNG k-ε in the broadband noise region.

Figure 8(a) and Figure 8(b) represent the calculated power spectrum from the LES and RNG k-ε with the same acoustic model at 6,500 Hz. From these figures, it can be seen that the calculated power spectrum on the surfaces of the blade tips is higher than the other areas. Thus, these surfaces are the dominant BPF noise source. Moreover, the power spectrum calculated by the LES is considerably higher than the power spectrum predicted by the RNG k-ε. This difference in power spectrum results in a greater power of noise source as well as a higher amplitude of SPL at the same measurement point. This finding obviously shows a good agreement with the predicted SPL at the BPF as shown in Fig. 6.

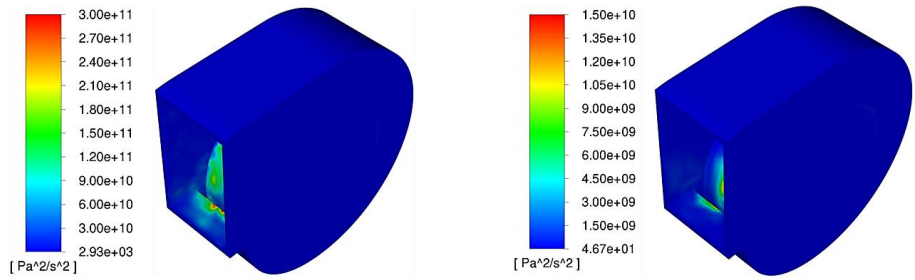

(a) LES at 2,000 Hz (b) RNG k-ε at 2,000 Hz

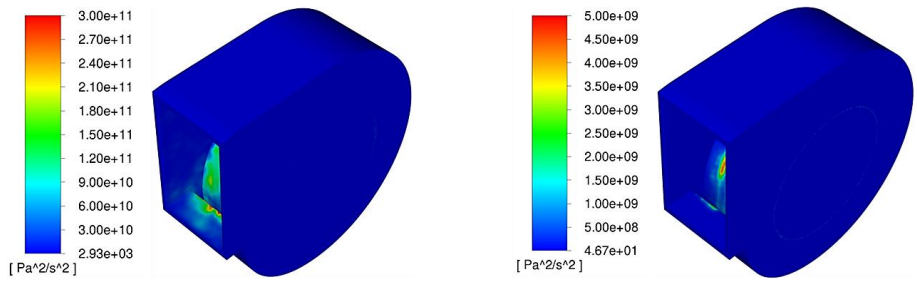

(c) LES at 4,000 Hz (d) RNG k-ε at 4,000 Hz

Fig. 7. The sample of the calculated spectrum in the broadband noise region.

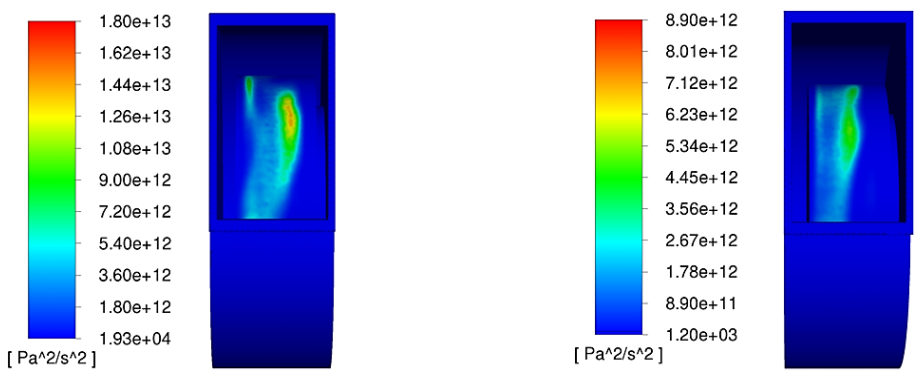

(a) LES at 6,500 Hz (b) RNG k-ε at 6,500 Hz

Fig. 8. The calculated spectrum at the BPF.

6. Conclusion

In this study, the characteristic of aerodynamic noise and the dominant noise source of the low Mach number centrifugal fan are investigated through the numerical approach. In addition, the experiment is set to validate the numerical study. The main conclusions of this study are summarized as follows.

1. The LES coupled with the acoustic model can provide a more accurate noise prediction result than the RNG k-ε coupled with the same acoustic model.
2. The overall SPL of the fan noise predicted from LES coupled with the acoustic model is 70 dBA, which is promising to the measurement result.
3. The surfaces of blade tips are the dominant BPF noise source, while the impeller and volute tongue surfaces are the main broadband noise source.
4. The configuration of fan noise measurement, which is used in this study fails to capture the characteristics of BPF noise.

Acknowledgement

The authors gratefully thank Mr. Thoranin Oonariya and Mr. Jiraphan Inthian from the iRAP Robot community; for accommodating in the 3D modelling procedure. This work is funded by the Program Management Unit for Human Resources & Institutional Development, Research, and Innovation through the Research Project of Tripartite Education System Using Work Based Learning.

References

[1] Neise W. Noise reduction in centrifugal fans: a literature survey. J Sound Vib. 1976;45(3):375-403.
[2] Neise W. Review of noise reduction methods for centrifugal fans. J Eng Ind. 1982;104(2):151-161.
[3] Ohta Y, Outa E. Noise reduction of blade-passing frequency components in a centrifugal blower. Proceedings of the ASME Turbo Expo; 2004 Jun 14-17; Vienna, Austria. New York: ASME. p. 1705-1714.
[4] Velarde-Suárez S, Ballesteros-Tajadura R, Pablo Hurtado-Cruz J, Santolaria-Morros C. Experimental determination of the tonal noise sources in a centrifugal fan. J Sound Vib. 2006;295(3-5):781-796.
[5] Heo S, Cheong C, Kim TH. Development of low-noise centrifugal fans for a refrigerator using inclined S-shaped trailing edge. Int J Refrig. 2011;34(8):2076-2091.
[6] Zhang J, Chu W, Zhang H, Wu Y, Dong X. Numerical and experimental investigations of the unsteady aerodynamics and aero-acoustics characteristics of a backward curved blade centrifugal fan. Appl Acoust. 2016;110:256-267.
[7] Marsan A, Moreau S. Aeroacoustic analysis of the tonal noise of a large-scale radial blower. J Fluids Eng. 2018;140(2):1-8.
[8] Wu L, Liu X, Wang M. Effects of bionic volute tongue on aerodynamic performance and noise characteristics of centrifugal fan used in the air-conditioner. J Bionic Eng. 2020;17(4):780-792.
[9] Chen J, He Y, Gui L, Wang C, Chen L, Li Y. Aerodynamic noise prediction of a centrifugal fan considering the volute effect using IBEM. Applied Acoust. 2018;132:182-190.
[10] Yang ZD, Gu ZQ, Wang YP, Yan JR, Yang XT. Prediction and optimization of aerodynamic noise in an automotive air conditioning centrifugal fan. J Cent South Univ. 2013;20(5):1245-1253.
[11] Kim JS, Jeong UC, Kim DW, Han SY, Oh JE. Optimization of sirocco fan blade to reduce noise of air purifier using a metamodel and evolutionary algorithm. Applied Acoust. 2015;89:254-266.
[12] Zore K, Parkhi G, Sasanapuri B, Varghese A. Ansys mosaic poly-hexcore mesh for high-lift aircraft configuration. 21st Annual CFD Symposium; 2019 Aug 8-9; Bangalore, India. p. 1-11.
[13] Lighthill MJ. On sound generated aerodynamically I. General theory. Proc R Soc Lond A. 1952;211(1107):564-587.
[14] Lighthill MJ. On sound generated aerodynamically II. Turbulence as a source of sound. Proc R Soc Lond A. 1954;222(1148):1-32.
[15] Ffowcs Williams JE, Hawkings DL, Lighthill MJ. Sound generation by turbulence and surfaces in arbitrary motion. Philos Trans Royal Soc A. 1969;264(1151):321-342.
[16] Howe MS. Theory of vortex sound. Cambridge: Cambridge University Press; 2002.
[17] ISO. ISO 3745:2012: Acoustics -- determination of sound power levels and sound energy levels of noise sources using sound pressure -- precision methods for anechoic rooms and hemi-anechoic rooms. Geneva: ISO; 2012.
[18] Meyer A, Döbler D, Hambrecht J, Matern M. Acoustic mapping on three-dimensional models. Proceedings of the 12th International Conference on Computer Systems and Technologies; 2011 Jun 16-17; Vienna, Austria. p. 216-220.